# Three-dimensional Heisenberg critical behavior in the highly disordered dilute ferromagnetic semiconductor (Ga,Mn)As

M. Wang,* R. A. Marshall, K. W. Edmonds, A. W. Rushforth, R. P. Campion, and B. L. Gallagher
*School of Physics and Astronomy, University of Nottingham, University Park, Nottingham NG7 2RD, United Kingdom*
(Received 24 September 2015; revised manuscript received 29 February 2016; published 16 May 2016)

We present detailed studies of critical behavior in the strongly site-disordered dilute ferromagnetic semiconductor (Ga,Mn)As. (Ga,Mn)As has a low saturation magnetization and relatively strong magnetocrystalline anisotropy. This combination of properties inhibits domain formation, thus removing a principal experimental difficulty in determining the critical coefficients $\beta$ and $\gamma$. We find that there are still a large number of problems to overcome in terms of measurement procedures and methods of analysis. In particular, the combined effects of disorder and inhomogeneity limit the accessible critical region. However, we find that accurate and reproducible values of the critical exponents $\beta$ and $\gamma$ can be obtained from Kouvel-Fisher plots of remanent magnetization and magnetic susceptibility for our (Ga,Mn)As samples. The values of $\beta$ and $\gamma$ obtained are consistent with those of the three-dimensional Heisenberg class, despite the very strong disorder present in this system, and they are inconsistent with mean field behavior. Log-log plots of $M(H)$ data for our samples are consistent with the three-dimensional Heisenberg value of the critical exponent $\delta$, but accurate values of $\delta$ could not be obtained for our samples from these plots. We also find that accurate values of the critical exponent $\alpha$ could not be obtained by fitting to the measured temperature derivative of resistivity for our samples. We find that modified Arrott plots and scaling plots are not a practical way to determine the universality class or critical exponents, though they are found to be in better agreement with three-dimensional Heisenberg values than mean field values. Below the critical temperature range, we find that the magnetization shows power-law behavior down to a reduced temperature of $t \sim 0.5$, with a critical exponent $\beta \sim 0.4$, a value appreciably lower than the mean field value of $\beta = 0.5$. At lower temperatures, Bloch 3/2 law behavior is observed due to magnons.

DOI: 10.1103/PhysRevB.93.184417

## I. INTRODUCTION

Close to the critical point of second-order phase transitions, such as the ferromagnetic-paramagnetic transition, power-law relationships between the thermodynamic variables of the system are observed. The critical power-law exponents depend on the symmetry and dimensionality of the system and on the symmetry and dimensionality of the order parameter. The symmetry and dimensionality are considered "relevant parameters" [1]. The critical exponents are insensitive to the microscopic details of the system (irrelevant parameters). The range of the interactions driving the phase transition is generally a relevant parameter. Diverse examples of second-order phase transitions observed in very different physical systems are found to belong to a relatively small number of universality classes. The universality classes are named after simple model systems that have the relevant parameters characterizing the universality class. The three-dimensional Heisenberg model considers three-dimensional vector magnetic moments interacting on a three-dimensional lattice with "short-range" interactions. Often, numerical simulations are done considering only nearest neighbor interactions, but the same universal behavior is obtained when the interaction range is beyond nearest neighbor, provided that the strength of the interaction decreases sufficiently rapidly with distance [2,3].

The renormalization group theoretical result known as the Harris criterion [4] shows that the three-dimensional Heisenberg critical exponents should be independent of disorder. This has been verified by several theoretical and experimental studies [5,6]. However, these same studies show that increasing disorder reduces the range around the critical temperature over which critical behavior can be observed. This leads to difficulties for both numerical simulations and experimental studies. Generally, theoretical and experimental studies have focused on relatively weak disorder [5].

Priour and Das Sarma [7] considered the strongly disordered case theoretically. They focused on (Ga,Mn)As as a model strongly disordered system. (Ga,Mn)As is a dilute magnetic semiconductor in which several percent of Mn substitutes for Ga. Mn is believed to substitute randomly for Ga in the lattice, leading to strong site disorder. Based on a model RKKY interaction with parameters consistent with the measured properties of (Ga,Mn)As, Priour and Das Sarma concluded that only nearest neighbor interactions needed to be considered, since the damping length is comparable with the lattice constant. Despite the strong disorder, the numerical calculations obtained three-dimensional Heisenberg behavior, but only very close to the Curie temperature ($T_C$).

(Ga,Mn)As, one of the most interesting and widely studied dilute magnetic semiconductors [8–11], is a model system that has been used to demonstrate a variety of novel phenomena during the last 20 years, such as gateable ferromagnetism [12], tunneling anisotropic magnetoresistance [13], current-induced domain wall motion [14], strain control of domain wall motion [15], and spin injection [16]. Despite the values of the highest Curie temperatures ($T_C$) achieved being well below room temperature [17–19], it is a valuable test ground for spintronics applications. Ferromagnetism in (Ga,Mn)As is due to the coupling of the dilute magnetic moments via delocalized holes. The Mn dopant is an acceptor when it substitutes for Ga and

*Current address: London Centre for Nanotechnology, University College London, 17-19 Gordon Street, London WC1H 0AH, United Kingdom.

 

provides both the local moments and the holes. Since it is a dilute ferromagnet, with Mn randomly substituting for Ga on the Ga lattice sites, this material is an extreme example of a disordered ferromagnetic system.

There have been several studies of critical behavior in (Ga,Mn)As. Most of these have focused on the critical contribution to the resistivity close to $T_C$ [20]. In dense moment ferromagnetic semiconductors, the moment density is much larger than the carrier density, and only long-wavelength spin fluctuations scatter carriers effectively. This leads to the resistivity having a peak at $T_C$ [21]. In dilute ferromagnetic semiconductors such as (Ga,Mn)As [18,22] and ferromagnetic metals [23], the carrier and moment densities are comparable. This leads to the temperature derivative of resistance having a peak at $T_C$, which has the same functional form as that of the specific heat [24]. A few experimental studies have tried to determine critical exponents for (Ga,Mn)As [25–28], and, as discussed later, these have generally produced imprecise and contradictory results. Stefanowicz *et al.* [29] carried out a detailed study of critical behavior in the related dilute ferromagnetic semiconductor (Ga,Mn)N. They found that inhomogeneity played a major role in this material leading to temperature-dependent "effective critical exponents."

(Ga,Mn)As has several properties that make it well suited to the study of critical behavior at the ferromagnetic-paramagnetic transition. (Ga,Mn)As layers grown by molecular beam epitaxy (MBE) on GaAs substrates can have very high crystalline quality. They generally show excellent micromagnetic properties that are well understood on the basis of both phenomenological and microscopic theories [30]. The low moment density of (Ga,Mn)As makes shape anisotropy very weak, and the relatively strong spin-orbit coupling leads to magnetocrystalline anisotropy dominating the magnetic behavior. (Ga,Mn)As epilayers, grown by MBE on GaAs, have in-plane compressive strain. This breaks the cubic symmetry, leading to biaxial ⟨100⟩ in-plane easy axes in most (Ga,Mn)As materials at low temperature. (Ga,Mn)As epilayers grown on GaAs also have a competing $[1\bar{1}0]$ in-plane uniaxial easy axis for which several explanations have been proposed [31]. For typical (Ga,Mn)As materials with relatively low Mn concentrations, one observes a smooth transition from biaxial ⟨100⟩ in-plane easy axes to a $[1\bar{1}0]$ in-plane uniaxial easy axis with increasing temperature [32]. However, materials with high Mn concentration and high $T_C$, such as those used in the present studies, show strong uniaxial behavior at all temperatures. Together, these properties lead to the samples studied behaving as single domain uniaxial magnets. This is particularly beneficial for the study of the critical behavior of the magnetization, since domain formation is suppressed.

Here, we present a detailed study of the critical behavior of the magnetic properties of high quality, high homogeneity, uniaxial (Ga,Mn)As close to $T_C$. Within relatively small experimental uncertainties, we observe three-dimensional Heisenberg behavior despite the very strong disorder.

## II. POWER LAWS AND THE CRITICAL TEMPERATURE REGION

Close to $T_C$, all the magnetic properties of ferromagnetic materials are determined by critical fluctuations and show power-law behavior [33]. It is useful to introduce the reduced temperature $t = (1 - T/T_C)$, the reduced magnetic field $h = \mu_0\mu_B H/k_B T_C$, and the reduced magnetization $m$, which is the magnetization divided by the $T = 0$ saturation magnetization. In the critical region just below a ferromagnetic/paramagnetic transition ($t \ll 1$), for $h = 0$, the reduced magnetization is given by

$$m \propto t^{\beta}. \tag{1}$$

Just above $T_C$, ($-t \ll 1$), the magnetic susceptibility, $\chi \propto m/h$, in the limit $h \to 0$, is given by

$$\chi \propto m/h \propto (-t)^{-\gamma}. \tag{2}$$

At $T_C$ ($t = 0$), the magnetization, in the limit $h \to 0$, is given by

$$m \propto h^{1/\delta}. \tag{3}$$

The magnetic contribution to the specific heat close to $T_C$, ($|t| \ll 1$), for $h = 0$, is given by

$$C_M \propto |t|^{-\alpha}. \tag{4}$$

As discussed in Sec. I, in dilute ferromagnetic semiconductors such as (Ga,Mn)As [18] and ferromagnetic metals [23], the temperature derivative of resistance close to $T_C$ should have the same power-law behavior as that of the specific heat [24].

The specific values of the critical exponents are characteristic of the universality class. For mean field behavior, $\beta = 0.5, \gamma = 1, \delta = 3$, and $\alpha = 0$. The calculation of accurate exponent values is challenging for most other classes, but accurate values of $\beta = 0.369$, $\gamma = 1.396$, $\delta = 4.783$, and $\alpha = -0.133$ have been obtained for the three-dimensional Heisenberg universality class [33].

The critical exponents are not independent. From critical scaling analysis [1,33], it is established that

$$\delta = 1 + \frac{\gamma}{\beta}, \tag{5}$$

and

$$\alpha = 2(1 - \beta) - \gamma, \tag{6}$$

and that the magnetic thermodynamic variables must be related by the equation

$$\frac{m(h,t)}{t^{\beta}} = f_{\pm}\left(\frac{h}{t^{\beta+\gamma}}\right), \tag{7}$$

where $f_{\pm}$ are two scaling functions for temperatures above and below $T_C$, respectively.

Equations (1) to (3) are consistent with the approximate equation of state first proposed by Arrott and Noakes [34] for the limit of small $t$, $m$, and $h/m$ [33]:

$$\left(\frac{h}{m}\right)^{1/\gamma} = at + bm^{1/\beta}, \tag{8}$$

where $a$ and $b$ are assumed to be temperature-independent coefficients related to the critical amplitudes. This equation of state was originally proposed as a partially empirical expression that fitted to earlier magnetization measurements on nickel, for which the critical exponents are close to the three-dimensional Heisenberg values. Equation (8) reduces to

Eq. (1) for $H \to 0$, Eq. (2) for $M \to 0$, and Eq. (3) for $t = 0$. It is also consistent with Eqs. (5) and (7). For the mean field exponents, Eq. (8) is

$$\left(\frac{h}{m}\right) = at + bm^2. \tag{9}$$

The critical exponents $\beta$ and $\gamma$ are only exact in the limit of "small" $t$ (the critical region), even in the absence of disorder. For the three-dimensional Heisenberg class, disorder does not modify these exponents, but it reduces the extent of the critical region. In experimental studies of a range of disordered ferromagnetic materials showing three-dimensional Heisenberg behavior, it was found that the critical region is of the order of a few percent of $T_C$ [5]. Trying to obtain critical exponents from data more than a few percent away from $T_C$ may lead to apparent deviations from the true critical exponents. This sets an upper limit on $|t|$, above which accurate critical exponents cannot be obtained.

Additionally in experimental studies, there is the particular problem that there will always be some large length scale inhomogeneity and corresponding variation of $T_C$ in real samples. This removes the singularities at "$T_C$" and produces apparent deviations from power-law behavior (see for example [35]). This sets a lower limit on $|t|$, below which accurate values of the critical exponents $\beta$, $\gamma$, and $\alpha$ cannot be obtained. It also implies that determining $\delta$ at "$T_C$" could be problematic.

Hence, for disordered ferromagnetic materials with significant inhomogeneity, it may not be possible to experimentally obtain the true critical exponents. As discussed below, this can potentially be a serious issue for (Ga,Mn)As materials.

## III. DATA ANALYSIS METHODS

### A. Log-log plots

One can attempt to obtain the power-law exponents for the magnetization and susceptibility by simply plotting the appropriate data set as a $\log(M)$ ($\log(m)$) or $\log(\chi)$ vs $\log|t|$ graph and taking the gradient close to $T_C$ as the exponent. Unfortunately, this method immediately runs into a number of problems that are not easily resolved. The main problem associated with this method is that one needs to know $T_C$ to calculate $t$.

While theoretically remanent magnetization should fall to zero at $T_C$, real measurements always display a tail "above $T_C$" due to sample inhomogeneity and the presence of finite magnetic fields arising from Earth's field and small remanent fields within magnetometer coils. The calculated exponent values are very sensitive to the value of $T_C$ used, and we find in our studies of (Ga,Mn)As that changing $T_C$ by $\sim 0.5\%$ using log-log plots can easily shift the inferred exponents between values expected for different universality classes.

Often when log-log plots are used, no attempt is made to independently obtain $T_C$, and both the exponent and the $T_C$ value are used as free fitting parameters to obtain the best straight-line behavior, or an arbitrary value of $T_C$ is chosen. From our studies of (Ga,Mn)As, we find that this can be very misleading and introduce large uncertainties that are hard to quantify.

Equation (3) suggests that one can obtain the critical exponent $\delta$ from a plot of $\log(M)$ against $\log(H)$ (or $\log(m)$ against $\log(h)$) at $T_C$. However, this requires the value of $T_C$ to be accurately known. In practice, the value of the critical exponent $\delta$ obtained can be a rapidly varying function of the $T_C$ used, and so, in the absence of some independent means of measuring $T_C$, one anticipates that obtaining values of the exponent $\delta$ in this way will not give reliable values.

### B. Arrott-Noakes plots

Often the $T_C$ values required to make the log-log plots are obtained experimentally using standard or modified Arrott plots [36]. Arrott plots assume that the equation of state (8) is correct. Plotting $m^{1/\beta}$ against $(h/m)^{1/\gamma}$ should then give parallel straight lines for each $t$, with that for $t = 0$ passing through the origin. However, to make such a plot, one must *assume* the exponent values. Given this requirement, the log-log plot plus Arrott plots approach is not a viable option when studying the critical phenomena because each of the steps requires the result of the other. The only real use for the modified Arrott plots in this case is therefore as a $T_C$ consistency check after the determination of $\beta$ and $\gamma$. Arrott plots of this type have been used to obtain $T_C$ values for (Ga,Mn)As samples [37], assuming mean field exponent values without any justification.

### C. Scaling plots

In principle, Eq. (7) can be used to find the critical exponent from measured $M(H,T)$ ($m(h,t)$) data. Plotting $t(h,t)/t^{\beta}$ as a function of $h/t^{\beta+\gamma}$ should lead to all data falling onto one curve above $T_C$ and one different curve below $T_C$ for the correct $\beta$ and $\gamma$ values. However, using $T_C$, $\beta$, and $\gamma$ as fitting parameters in this type of plot is not, in practice, a viable way to obtain their values. In this respect, such scaling plots present the same difficulties as the Arrott-Noakes method. However, such plots do not rely on a specific approximate equation of state and so may have a larger range of validity. Such plots can still be useful for checking the consistency of the parameters obtained from other methods.

### D. Kouvel-Fisher plots

An alternative and relatively simple method to avoid the problems of log-log plots, Arrott plots, and scaling plots is to use Kouvel-Fisher plots [38]. From Eqs. (1) and (2) and the definition of reduced magnetization, it follows that

$$\left(\frac{\mathrm{d}\ln M}{\mathrm{d}T}\right)^{-1} = -\frac{1}{\beta}(T_C - T), \tag{10}$$

and

$$\left(\frac{\mathrm{d}\ln \chi}{\mathrm{d}T}\right)^{-1} = -\frac{1}{\gamma}(T - T_C). \tag{11}$$

Therefore, plots of $(\mathrm{d}\ln M/\mathrm{d}T)^{-1}$ or $(\mathrm{d}\ln\chi/\mathrm{d}T)^{-1}$ against $T$ yield the $\beta$ and $\gamma$ values from the gradients and the value of the $T_C$ from the intercept on the $T$ axis. These Kouvel-Fisher plots are established as the best approach for the determination of the critical temperature.

## IV. SAMPLES AND EXPERIMENTAL METHODS

### A. Materials and samples

The samples studied were 25-nm-thick (Ga,Mn)As layers grown on semi-insulating GaAs(001) substrates by low-temperature molecular beam epitaxy, with nominal manganese concentration from 6 to 12%. The growth procedures used produce materials with highly uniform substitutional Mn concentration [17] and excellent micromagnetic properties [39]. As-grown (Ga,Mn)As epilayers have relatively low $T_C$ due to self-compensation by interstitial Mn. However, the interstitial Mn is relatively mobile and can be removed by low temperature annealing [40] to produce material in which the carrier and moment compensation is very low [41]. As-grown (Ga,Mn)As has a gradient in the interstitial Mn concentration in the growth direction due to partial annealing during MBE growth and a corresponding gradient in $T_C$ [42]. The samples used in these studies were annealed in air for 48 hours at 180°C, a procedure which has been shown to increase the homogeneity [43] and the critical temperature $T_C$ [17].

### B. Magnetic measurements

The magnetic properties of the (Ga,Mn)As samples were measured in a Quantum Design superconducting quantum interference device (SQUID) magnetometer with the reciprocating sample option (RSO). It is obviously important to accurately know the applied field in $M(H)$ measurements. It is also crucially important to minimize background magnetic fields in measurements of remanent magnetization, since these can significantly modify the behavior close to $T_C$. The magnetization vs temperature data of Fig. 1 show that the sensitivity to small applied fields is relatively low if one is more than about 1 K above or below $T_C$, but that a magnetic field as small as 1 Oe can dramatically change the magnetization very close to the Curie temperature. One therefore needs to minimize trapped flux within the superconducting coils of the SQUID system. To do so, the applied magnetic field during the remanent magnetization measurements has to be as small as possible, but the field needs to be large enough to saturate the samples' magnetization. Magnetic fields of 300 Oe or less were therefore used throughout the measurements. Oscillatory demagnetization of the magnet coils was also carried out between data set measurements and when changing samples. Even with these precautions, it is not possible to totally eliminate trapped flux in a superconducting magnet system. For the sample of Fig. 1, we obtained $T_C = 183.5$ K (see Sec. V F). The behavior of $m(T)$ for nominally zero applied fields suggests that fields of a fraction of an Oersted were present.

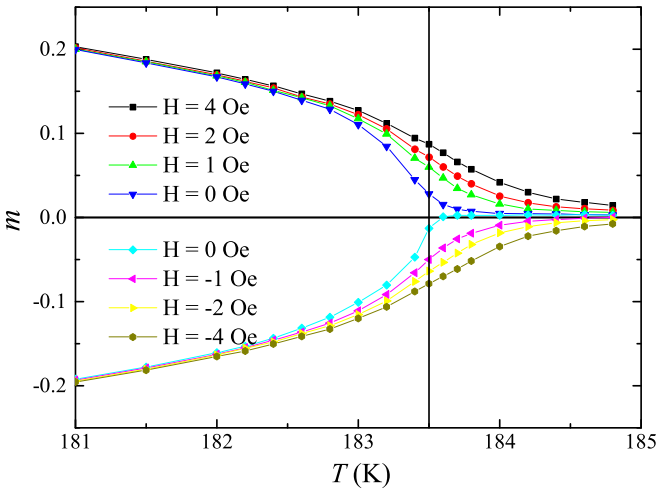


FIG. 1. Measured reduced magnetization (i.e., the magnetization divided by the $T = 0$ saturation magnetization) of the 12% (Ga,Mn)As sample for small applied magnetic fields. The value of $T_C$ we obtain for this sample from remanent magnetization Kouvel-Fisher plots is 183.5 K.

Because the diamagnetic signal from the GaAs substrate on which the (Ga,Mn)As epilayers were grown can give a large contribution to the total magnetic moment and shift the magnetic susceptibility, it is necessary to remove this background precisely in critical behavior studies. To minimize the diamagnetic background from the substrate and sample holder, the sample was mounted on a thin strip of silicon and abutted on either side with strips of GaAs of the same thickness and width as the substrate [Fig. 2(a)]. Both the silicon mount and the GaAs strips extend much further than the position of the detection coils of the SQUID magnetometer. This leads to the magnetic flux due to substrate and sample mount that is detected by the magnetometer being very small. As an example, Fig. 2(b) shows the magnetization vs temperature on cooling in a 300 Oe applied field, with and without the GaAs strips in place. The negative shift of the black points is the result of the substrate diamagnetic background. This is almost completely removed when the GaAs strips are used.

Detailed measurements and analysis were performed on two samples, with nominal Mn concentrations of 11% and 12%, respectively. The approximate $T_C$ value was established in initial measurements. Remanent magnetization was measured by first field cooling from room temperature to 2 K at 300 Oe, and then measuring the sample magnetization while warming in zero applied field with a 1 K temperature step. A temperature step size of 0.1 K was used from 10 K below the established approximate $T_C$ value to increase the number of data points over the critical region and to improve thermal equilibrium in this region. Kouvel-Fisher analysis of the data was then used to obtain the $\beta$ critical exponent and $T_C$.

Two full sets of DC $M(H)$ hysteresis loop measurements were carried out on each sample. The first set was taken over a temperature range from just below the approximate $T_C$ up to 10 K above at intervals of 0.5 K. These were then used to calculate the susceptibility $\chi$ as a function of temperature by averaging both the up and down sweeps, and linearly fitting around $H = 0$. Both fit and sweep range of each measurement were increased with temperature, with a maximum sweep range of $\pm 200$ Oe from roughly 5 K above $T_C$. Kouvel-Fisher analysis of the susceptibility data was used to obtain the $\gamma$ critical exponent, and it also provided a consistency check on the value of $T_C$.

Further $M(H,T)$ measurements were taken at temperatures above and below the expected $T_C$ over a range of $\pm 3$ K and for magnetic fields up to $\pm 20$ Oe. In this case, rather than using a constant temperature step size, decreasing temperature intervals were used down to 0.1 K upon approaching the approximate $T_C$. These $M(H,T)$ data were used to produce standard and modified Arrott plots with the mean field and three-dimensional Heisenberg exponent values, respectively.

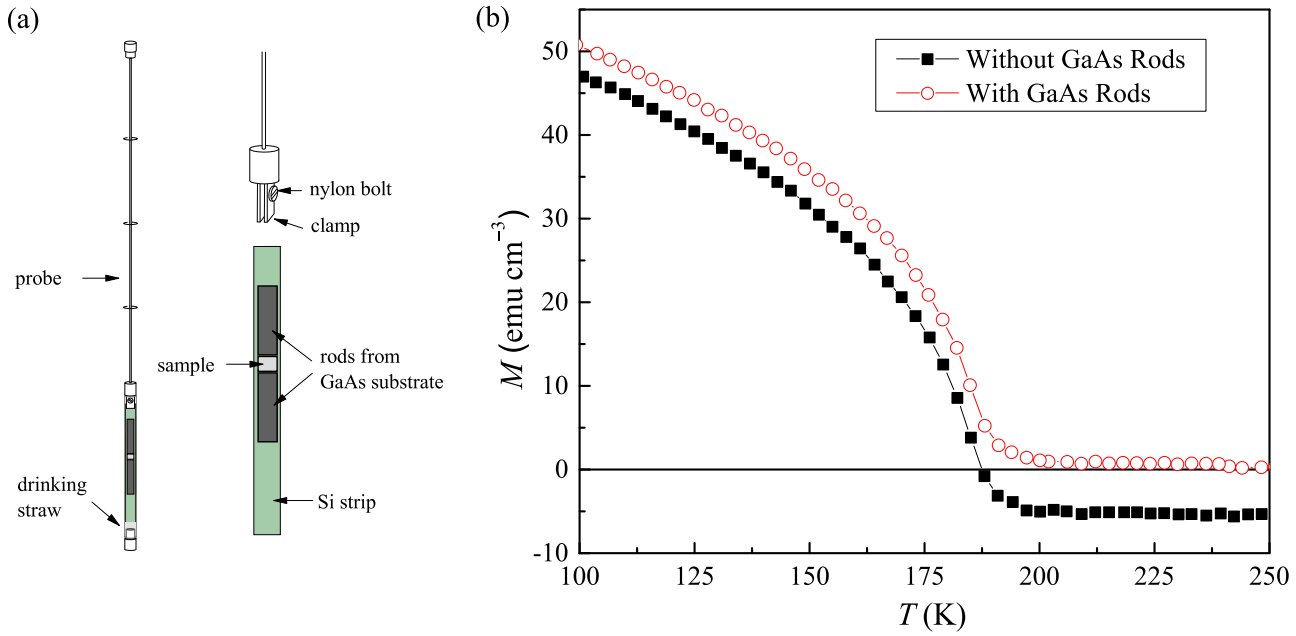


FIG. 2. (a) A diagram of the SQUID probe and the sample mounting. (b) Field-cooling data at 300 Oe for the 12% (Ga,Mn)As sample with (red) and without (black) the use of the additional GaAs rods to remove the negative diamagnetic background.

Linear fitting to each of the isotherms was then used to calculate a value of $T_C$ for both models. The same data sets were also used to try to obtain the critical exponent $\delta$ and to produce scaling plots with mean field and three-dimensional Heisenberg models with the relevant $T_C$ values obtained from the Arrott plots.

## V. RESULTS

In this section, we will present the results of detailed, high-resolution studies of two high-quality (Ga,Mn)As samples with Mn concentrations of 11% and 12%, respectively. We also present some results of lower-resolution studies of a large number of annealed samples with a wide range of Mn concentrations (from 6% to 12%) and $T_C$ values (from 117 K to 180 K).

### A. Measured remanent magnetization

Figures 3(a) and 3(b) show the temperature dependencies of the projected magnetization along the $[1\bar{1}0]$ crystalline axis measured on cooling through $T_C$ in a 300 Oe magnetic field, and then warming under zero applied field for the 12% and 11% Mn samples, respectively. Annealed (Ga,Mn)As materials with high Mn content have strong $[1\bar{1}0]$ uniaxial anisotropy, and they are in a single domain state after field cooling, so the total spontaneous magnetization is equal to the projection of remanent magnetization along the $[1\bar{1}0]$ easy axis. This can be seen from the comparison of the remnant and field-cooled measurements, which are almost identical, except very close to $T_C$.

### B. Measured remanent magnetization just below $T_C$: Obtaining the critical exponent $\beta$

The Kouvel-Fisher analysis was carried out on the remanent magnetization for both samples. Numerical differentiation was carried out using nearest neighbor least-squares smoothing to reduce the amplification of noise produced by the differentiation. Figures 3(c) and 3(d) show the Kouvel-Fisher plots with linear fitting performed over the reduced temperature ranges $0.025 > |t| > 0.005$ for the 12% and 11% Mn samples, respectively. This range was chosen because the Kouvel-Fisher plots are reasonably linear in this range. At larger $|t|$ (further below $T_C$), the data become much noisier, and, as discussed in Sec. V C, the plots become nonlinear. At lower $|t|$ (very close to $T_C$), the Kouvel-Fisher plots are very nonlinear, with a marked drop-off close to $T_C$. These apparent drop-offs and associated apparent increase in the exponent $\beta$ just below $T_C$ are the result of sample inhomogeneity [22]. Taking the observable critical range to be $0.025 > |t| > 0.005$ gives $\beta = 0.361 \pm 0.005$ and $0.373 \pm 0.007$, respectively, for the 12% and 11% samples. These values are consistent with the value of 0.369 predicted by the three-dimensional Heisenberg model [33] and inconsistent with the mean field value of 0.5. The corresponding values of $T_C$ are $183.7 \pm 0.1$ K and $169.0 \pm 0.1$ K. Figure 3(e) shows the Kouvel-Fisher plots for both samples shifted by their respective calculated $T_C$ values. The two data sets overlay very well in the range from $T_C$ down to about 8 K below $T_C$. Fitting to the combined data set in Fig. 3(e) over the range $0.025 > |t| > 0.005$ gives $\beta = 0.366 \pm 0.003$, i.e., a value close to the three-dimensional Heisenberg value with a small fitting uncertainty. However, as discussed below, one must also consider the influence of the fitting range used on the value obtained.

To test the sensitivity of the value of $\beta$ obtained from the Kouvel-Fisher plots, we show in Fig. 4 the effect of changing the reduced temperature ($t$) fitting range on the obtained value of $\beta$. The upper bound is fixed at $t_{upper} = 0.005$, and $\beta$ is plotted as a function of the value of the lower bound $t_{lower}$. Black squares and red circles are for the 12% and 11% samples, respectively. The horizontal dark blue line is

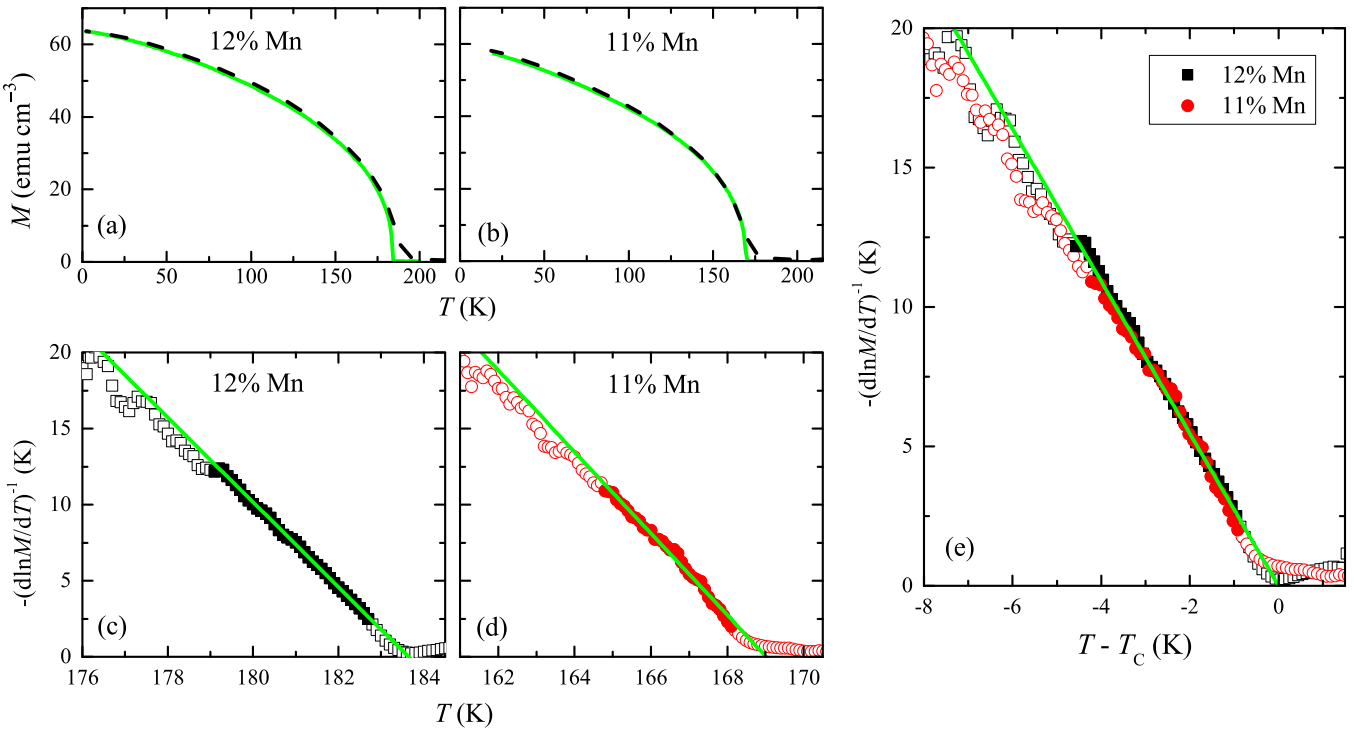


FIG. 3. (a, b) The projection of the temperature-dependent remanent (green solid line) and field-cooled (black dashed line) magnetization along the [1$\bar{1}$0] crystalline axis for the 12% and 11% Mn samples. (c, d) The Kouvel-Fisher plots of $(\mathrm{d}\ln M/\mathrm{d}T)^{-1}$ for the 12% and 11% Mn samples. The green lines are the linear fits to the data in the range $0.025 > |t| > 0.005$ (marked by filled symbols). (e) Combined Kouvel-Fisher plots for both samples using the $T_C$ values obtained from the individual plots of (c, d). The green line is the linear fit within the range $0.025 > |t| > 0.005$ for the combined data set.

the three-dimensional Heisenberg exponent $\beta = 0.369$. In the range $0.025 < t_{\mathrm{lower}} < 0.035$, there is a transition from the three-dimensional Heisenberg value to an apparent value of $\beta \sim 0.4$. As discussed in Sec. V C, this value is observed down to values of $T$ well below $T_C$ and well outside the critical range. For values of $t_{\mathrm{lower}} < 0.02$, the apparent value of $\beta$ decreases. However, as discussed in Sec. V E, this behavior is broadly consistent with that calculated for the Heisenberg exponent $\beta = 0.369$ in the presence of quite small degrees of inhomogeneity.

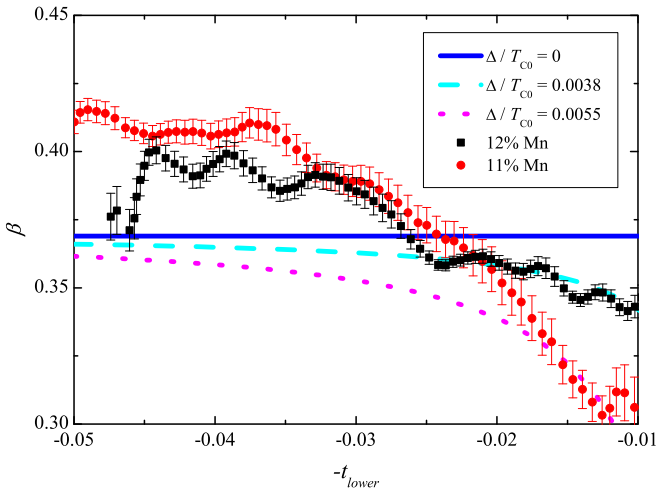


FIG. 4. Dependence of the value of $\beta$ obtained from Kouvel-Fisher plots on the lower bound of the fitting window. The upper bound is fixed at $t_{\mathrm{upper}} = 0.005$. Black squares and red circles are for the 12% and 11% samples, respectively. The horizontal dark blue line is the three-dimensional Heisenberg exponent $\beta = 0.369$. The light blue dashed line and purple dotted line are the behavior calculated for the Heisenberg exponent $\beta = 0.369$ using Eq. 13 for $\Delta/T_{C0}$ values of 0.0038 and 0.0055, respectively.

We also obtained $\beta$ values from Kouvel-Fisher analysis of lower-resolution remanent magnetization data for a large number of samples with a wide range of Mn concentrations. Figure 5 shows typical data for three different samples. Figure 6(a) is a histogram of the $\beta$ values. The distribution is quite wide, and there are a number of outliers. The red line is a Gaussian fit to the main peak, which gives a $\beta$ value of $0.36 \pm 0.01$. The mean of all the data gives a $\beta$ value of $0.37 \pm 0.02$. Both values are consistent with the value of 0.369 predicted by the three-dimensional Heisenberg model [33] and inconsistent with the mean field value of 0.5.

Figure 6(b) shows that no significant dependence of the apparent value of $\beta$ on the Mn concentration (or $T_C$, which increases monotonically with the Mn concentration for these samples) is observed.

### C. Measured remanent magnetization at lower temperatures

Figure 7 shows that at temperatures well below $T_C$, the Kouvel-Fisher plots are approximately linear down to $t \sim 0.5$. Fitting in this region gives an exponent $\beta \sim 0.4$. It is not clear why this behavior is observed, since one expects a

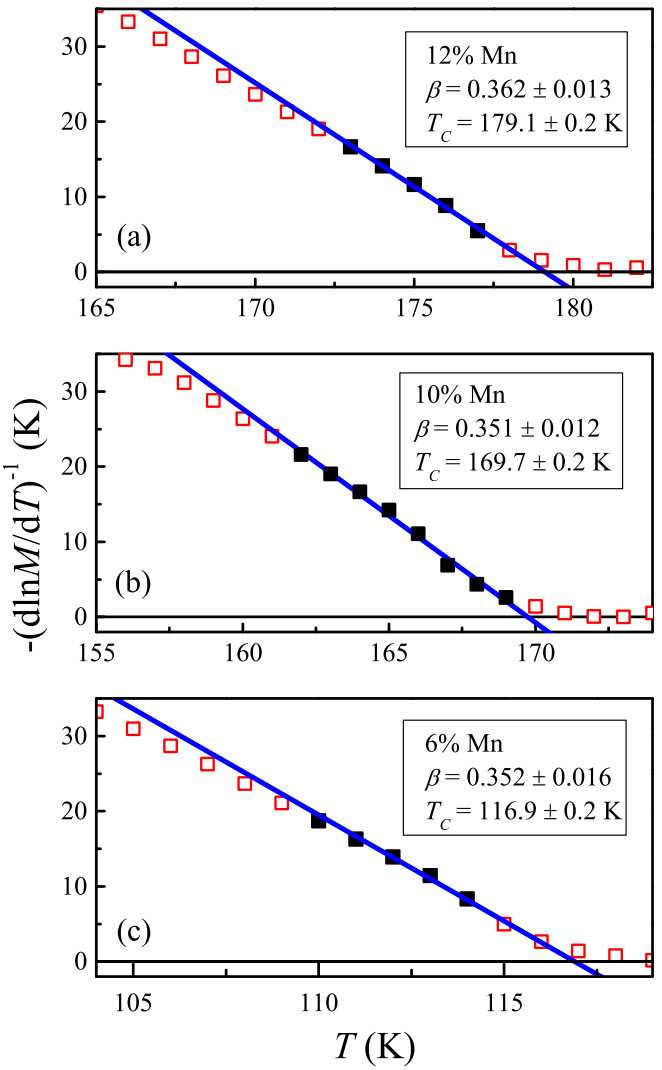


FIG. 5. Lower resolution remanent magnetization Kouvel-Fisher plots for samples with nominal Mn concentration of (a) 12%, (b) 10%, and (c) 6%. Fitting was performed to the data range indicated by filled squares. The blue lines are the resulting linear fits.

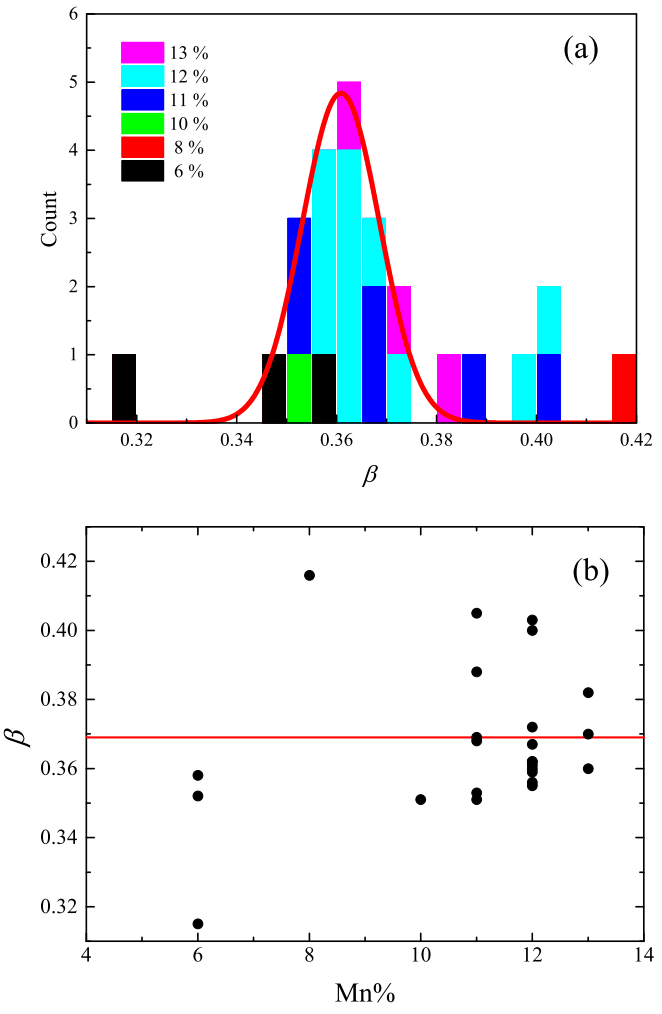


FIG. 6. (a) Histogram of $\beta$ values calculated from lower-resolution Kouvel-Fisher plots for (Ga,Mn)As samples with a range of Mn concentrations, layer thicknesses, and growth conditions. The Mn concentration is indicated in the color key. The red line is a Gaussian fit to the main peak, which gives a $\beta$ value of $0.36 \pm 0.01$. The mean of all the data gives a $\beta$ value of $0.37 \pm 0.02$. (b) Diagram showing the lack of a significant dependence of the obtained $b$ on the Mn concentration for these samples.

transition into mean field behavior with $\beta = 0.5$. Khazen *et al.* [26] obtained a similar value of $\beta$ from log-log plots of magnetization fitting down to $t = 0.35$ with a data point separation of 5 K. We conclude that the upper limit of the accessible critical range is $t \sim 0.025$. The value obtained by Khazen *et al.* is therefore consistent with the value we obtain below the critical range.

Below this temperature range, the Kouvel-Fisher plots become strongly nonlinear. For $T$ well below $T_C$, the effects of spin-wave excitations are expected to dominate, with the remanent magnetization following Bloch's 3/2 law [44]:

$$\frac{M(T) - M(0)}{M(0)} = AT^{3/2}, \tag{12}$$

where $A$ is a parameter related to the spin stiffness. Figure 8 shows $M/M_0$ vs $T^{3/2}$ plots of both the 11% and 12% Mn (Ga,Mn)As samples. It shows clear linear behavior below 50 K.

The low-temperature behavior of the magnetization was investigated for a series of (Ga,Mn)As samples by Sperl *et al.* [45]. It was reported that the normalized spin wave coefficient $A_{3/2} = AT_C^{3/2}$ is enhanced compared to conventional $3d$ ferromagnets. This was attributed to the effects of impurity disorder and spin clustering. For both the 11% and 12% samples, we obtain values of $A_{3/2}$ of around 0.6, which is consistent with the values obtained by Sperl *et al.* [45].

### D. Measured magnetic susceptibility just above $T_C$: Obtaining the critical exponent $\gamma$

Figures 9(a) and 9(b) show that the measured inverse susceptibilities are clearly not linear (mean-field-like). Figures 9(c) and 9(d) show the Kouvel-Fisher plots of the measured susceptibilities. Linear fitting over the temperature range $0.025 > |t| > 0.005$ gives values of $\gamma$ of $1.47 \pm 0.07$

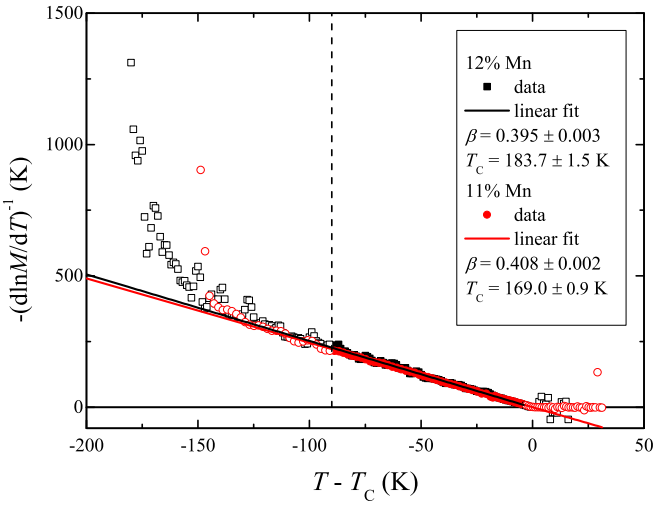


FIG. 7. Shifted Kouvel-Fisher plots of larger step-size remanent magnetization data over a wide temperature for 12% and 11% Mn samples. Linear fitting was performed in the range $-90\,\mathrm{K} < T - T_C < -3\,\mathrm{K}$.

and $1.51 \pm 0.10$ for the 12% and 11% Mn samples, respectively. These values are consistent with the value of 1.396 predicted by the three-dimensional Heisenberg model [33] and inconsistent with the mean field value of 1.0. The corresponding values of $T_C$ are $184.0 \pm 0.1$ K and $170.0 \pm 0.2$ K. These are $0.3 \pm 0.2$ K and $1.0 \pm 0.3$ K higher, respectively, than the values obtained from the remanent magnetization Kouvel-Fisher plots. The latter difference is clearly significant. How such discrepancies can arise due to inhomogeneity is discussed in Sec. V E. Figure 9(e) shows that the Kouvel-Fisher plots for the two samples shifted by their respective calculated $T_C$ values overlay very well in the range $0.025 > |t| > 0.005$, which we are taking to be the observable critical range. The value of $\gamma$ for the combined data set over this range of $|t|$ is $1.47 \pm 0.05$, a value consistent with the three-dimensional Heisenberg model. At higher temperatures, the susceptibility becomes very small and comparable with the resolution of the SQUID measurement system.

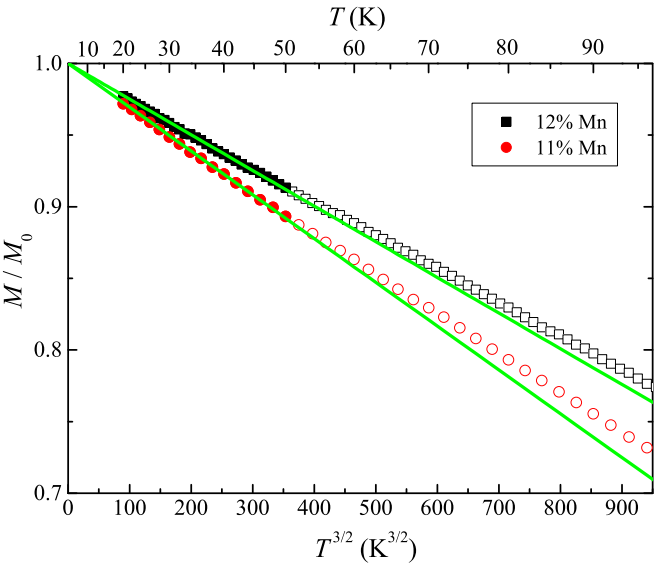


FIG. 8. $M/M_0$ against $T^{3/2}$ for 12% (squares) and 11% (triangles) samples. The green lines are the linear fit between 20 K and 50 K.

### E. The effects of inhomogeneity on the measured remanent magnetization and susceptibility

We have noted that, in real samples, there will always be some large length-scale inhomogeneity and a corresponding variation of $T_C$ that removes the singularities at "$T_C$" and sets a lower limit on $|t|$, below which accurate values of the critical exponents $\beta$ and $\gamma$ cannot be obtained. We now quantify these effects and compare the measured results to those expected in the presence of inhomogeneity.

The effect of broadening on $M(T)$ was modelled in an approach similar to that of Kuz'min and Tishin [35] and Stefanowicz *et al.* [29]. In these previous studies, a Gaussian distribution of magnetic impurities or $T_C$ was used. We have previously studied the distribution of $T_C$ values as a function of position on our MBE-grown wafers. We find that the samples, which are rotated during growth, have small variations of $T_C$ across a 2 inch (~5 cm) wafer, and that the variation is radial, due to small differences in the fluxes and substrate temperature between the center and edge of the wafer [17]. In this circumstance, we expect a small and approximately linear variation of $T_C$ across the 4-mm-sized samples used in this study. We therefore assume a rectangular distribution of $T_C$ with a half-width $\Delta$. $M(T)$ is then given by

$$M(T) = \frac{M_0}{2\Delta}\int_{T_{C0}-\Delta}^{T_{C0}+\Delta} f(T,T_C)\,dT_C, \tag{13}$$

where

$$f(T,T_C) = \left(1 - \frac{T}{T_C}\right)^{\beta} \quad \text{for} \quad T < T_C \text{ and } f(T,T_C) = 0 \quad \text{for} \quad T > T_C.$$

We find that the specific form of the $T_C$ distribution does not substantially influence the predicted behavior for small inhomogeneity (see below). Figure 10(a) shows calculated magnetization vs temperature, using the three-dimensional Heisenberg critical exponent $\beta = 0.369$ and the mean critical temperature $T_{C0} = 183.7$ K obtained from the Kouvel-Fisher plot for the 12% Mn sample, for various values of the broadening half-width $\Delta$. This indicates that the measured behavior of $M(T)$, close to $T_C$, for the 12% Mn sample is similar to that expected for a broadening of order $\Delta = 0.5$ K. The corresponding Kouvel-Fisher plots are shown in Fig. 10(b). This value of $\Delta$ corresponds to a value of $t = 0.003$.

The effect of inhomogeneity on the magnetic susceptibility can be similarly estimated using the same probability distribution of $T_C$ as in Eq. (13). Within this model, $\chi(T)$ is given by

$$\chi(T) = \frac{\chi_0}{2\Delta}\int_{T_{C0}-\Delta}^{T_{C0}+\Delta}\left(\frac{T}{T_C} - 1\right)^{-\gamma} dT_C, \tag{14}$$

where $\chi(T)$ is evaluated for $T > T_{C0} + \Delta$ to avoid the singularity at $T_C$ implied by this functional form. The susceptibility Kouvel-Fisher plots for various values of the broadening

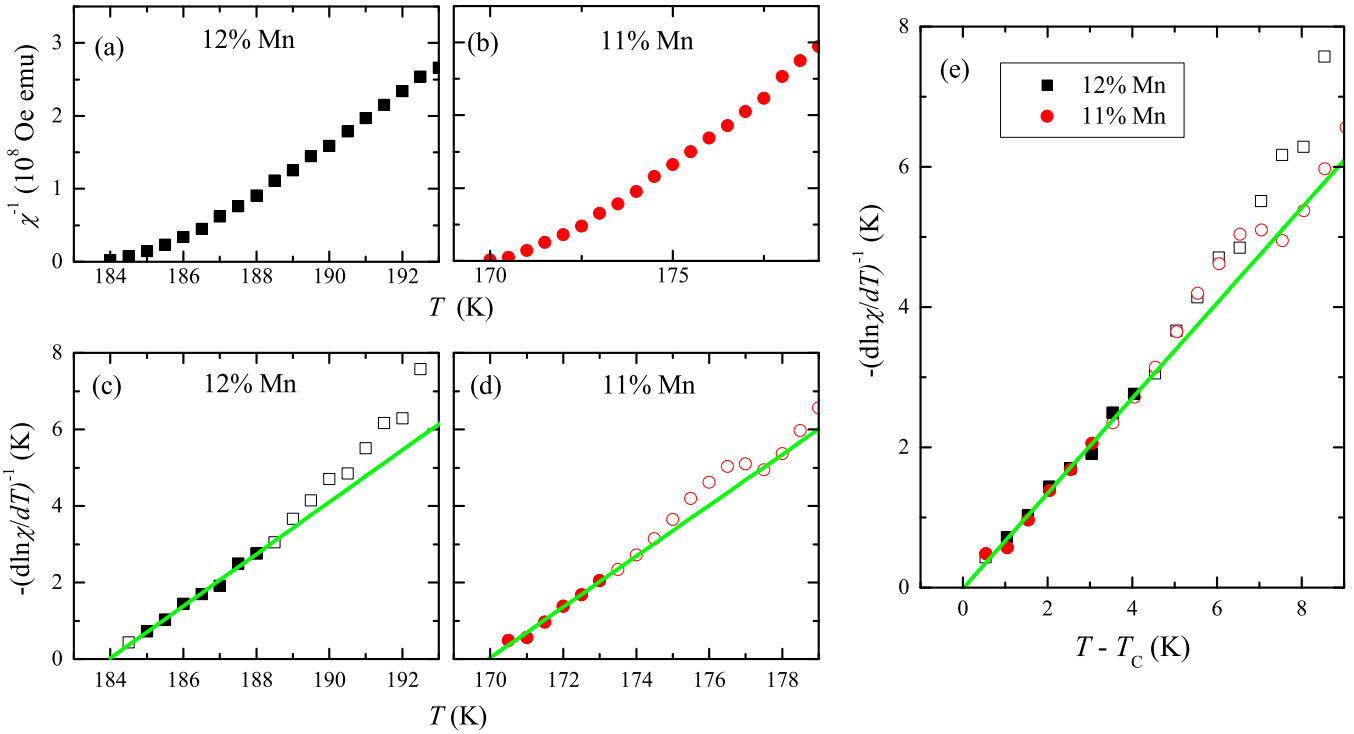


FIG. 9. (a, b) The measured inverse susceptibility for the 12% and 11% Mn samples. (c, d) The Kouvel-Fisher plots of $(\mathrm{d}\ln\chi/\mathrm{d}T)^{-1}$ for the 12% and 11% Mn samples. The green lines are the linear fits to the data in the range $0.025 > |t| > 0.005$ (marked by filled symbols). (e) Combined Kouvel-Fisher plots for both samples using the $T_C$ values obtained from the individual plots of (c, d). The green line is the linear fit within the range $0.025 > |t| > 0.005$ for the combined data set.

half-width $\Delta$, calculated using the three-dimensional Heisenberg exponent $\gamma = 1.396$ and a mean critical temperature $T_{C0} = 183.7$ K, are compared to the measured result for the 12% Mn sample in Fig. 11(a).

To illustrate the effects of inhomogeneity on the values of $T_C$ and the critical exponents obtained from Kouvel-Fisher plots, Eqs. (13) and (14) were evaluated for $T_{C0} = 183.7$ K, $\beta = 0.369$, and $\gamma = 1.396$, and $\Delta$ over the range 0–1.5 K. Figures 11(b) and 11(c) show the values of $T_C$, $\beta$, and $\gamma$ that result from fitting to the Kouvel-Fisher plots derived from the calculated $M(T)$ and $\chi(T)$. The fitting was performed over the range of $t = (1 - T/T_{C0})$ given by $0.005 < |t| < 0.025$. With increasing broadening, the fitted values of both the critical exponents, $\beta_{\mathrm{fit}}$ and $\gamma_{\mathrm{fit}}$, decrease from their true values, while the values of the critical temperature obtained from the magnetization and susceptibility Kouvel-Fisher plots, $T_{C,\mathrm{fit}}$, diverge from each other. This illustrates the importance of highly homogeneous samples when studying critical phenomena. The observed differences in $T_C$ between the magnetization and susceptibility data of $0.3 \pm 0.2$ K and $1.0 \pm 0.3$ K for the 12% and 11% samples, respectively, are consistent with broadening half-widths of $0.5 \pm 0.2$ K and $1.0 \pm 0.3$ K, respectively.

The dependence of the apparent $\beta$ on the lower limit of the $t$ fitting range for the calculated Kouvel-Fisher plots is shown in Fig. 4, together with the experimental data. As with the experimental curves, the upper limit of the fitting range was fixed at $t_{\mathrm{upper}} = -0.005$. Consistent with the experimental result, the apparent $\beta$ is below the real value of $\beta = 0.369$ used in the calculation, and it falls significantly as $|t_{\mathrm{lower}}|$ is reduced. Good agreement with the results for the 11% and 12% samples is found in the critical region (i.e., below $t \sim 0.025$) for relative broadenings of around $\Delta/T_{C0} = 0.006$ and $\Delta/T_{C0} = 0.004$, respectively. The precise dependence on inhomogeneity depends on the details of the broadening included in the calculation.

### F. Standard and modified Arrott plots

The measurements of $M(H,T)$ used to produce the Arrott plots of this section and the critical scaling plots of the next section were carried out several months after the measurements of remanent magnetization and susceptibility presented in Secs. V A–V E. For the 12% Mn sample, it was found that the $T_C$ value had reduced by about 0.2 K between these different sets of measurements. This is apparent in Fig. 12, where the remanent magnetization is shown for the earlier and later data sets. No significant shift was found for the 11% sample.

Figure 13 shows both standard mean field Arrott plots and modified Arrott plots (Arrott-Noakes plots) using three-dimensional Heisenberg exponents for the 12% and 11% Mn samples. The reduced magnetization, $m$, is the measured $M$ divided by $M(2\mathrm{K})$, and $h = \mu_0\mu_B H/k_B T_C$. These were produced by averaging the up and down $m(h)$ sweeps and the positive and negative field regions and then plotting $m^{1/\beta}$ against $(h/m)^{1/\gamma}$. First, it should be noted that since our data are measured close to $T_C$ for small applied fields, the basic conditions for the validity of these plots ($t$, $m$, and $h/m \ll 1$) are satisfied.

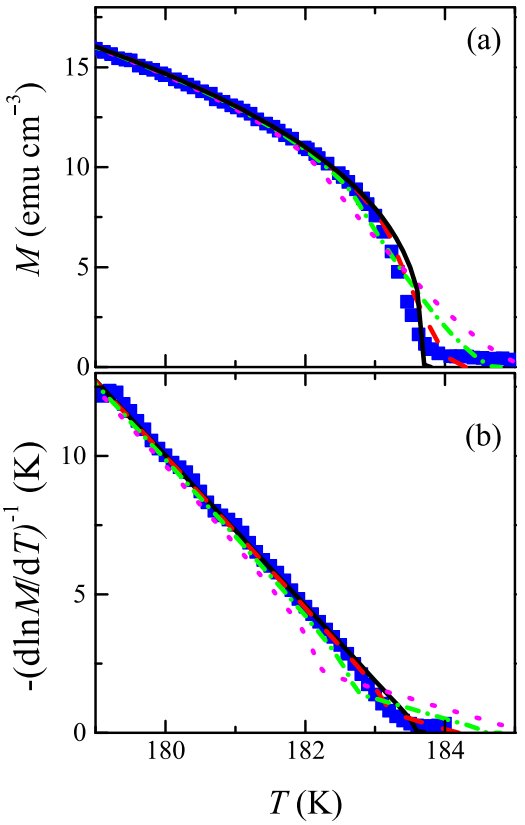


FIG. 10. (a) Experimental magnetization vs temperature for 12% Mn sample (squares) compared to calculated critical behavior for a rectangular broadening half-width $\Delta = 0$ (black continuous line), $\Delta = 0.5$ K (red dashed line), $\Delta = 1.0$ K (green dot-dashed line), and $\Delta = 1.5$ K (magenta dotted line). (b) Kouvel-Fisher plots for the data in (a).

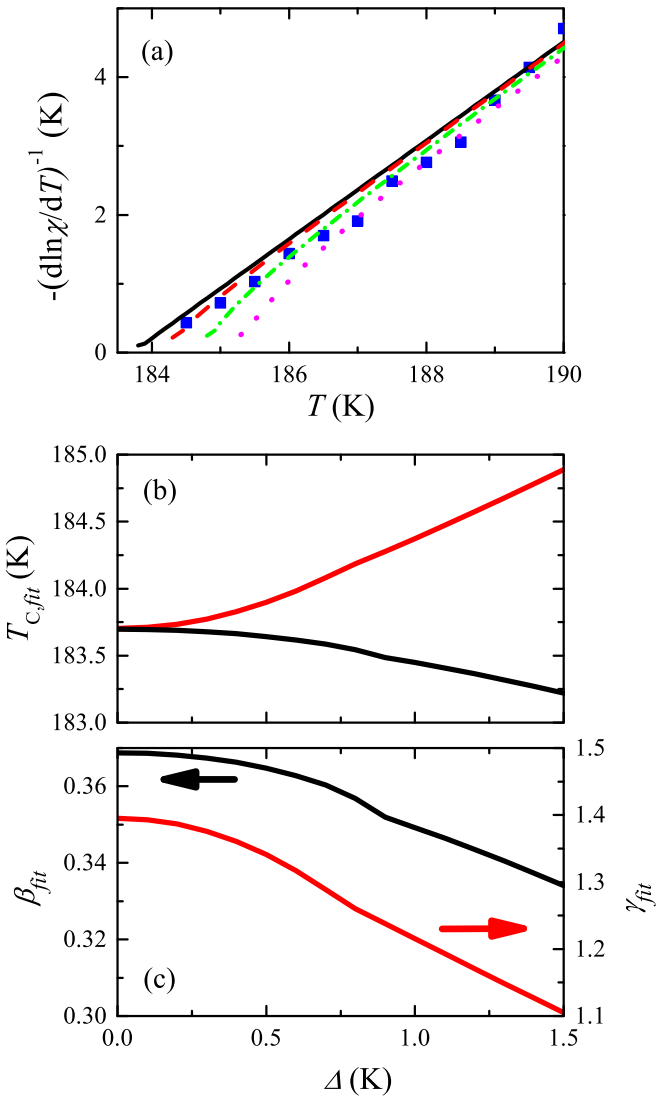


FIG. 11. (a) Kouvel-Fisher plot for the measured susceptibility of 12% Mn sample, compared to calculations for a rectangular broadening half-width $\Delta = 0$ (black continuous line), $\Delta = 0.5$ K (red dashed line), $\Delta = 1.0$ K (green dot-dashed line), and $\Delta = 1.5$ K (magenta dotted line). (b) $T_C$ extracted from the Kouvel-Fisher plots of the calculated critical behavior of the magnetization (black line) and susceptibility (red line) as a function of the rectangular broadening of half-width $\Delta$. (c) Critical exponents $\beta$ (black line, left axis) and $\gamma$ (red line, right axis) extracted from the calculated magnetization and susceptibility, respectively, vs $\Delta$.

It is clear from Fig. 13 that the measured data are in much better agreement with Eq. (8) with three-dimensional Heisenberg exponents than with the equivalent mean field, Eq. (9). We emphasize two important points about Fig. 13. First the plots using mean field exponents are significantly less linear than those using three-dimensional Heisenberg exponent values for both samples. In particular, while reasonable straight line fits to *all the data* are possible for the three-dimensional Heisenberg exponents, the behavior for the mean field exponents (the standard Arrott plots) is far from linear at small $h/m$. A superlinear fall in $m^2$ at small $h/m$ in standard Arrott plots is often ascribed to domain formation. However, linear behavior down to the smallest $h/m$ is observed in the modified Arrott plots, indicating that the nonlinearity at small $h/m$ in the standard Arrott plots is due to the non-mean-field-like critical exponents. Second, the modified Arrott plots show very little change in gradient below the expected Curie temperatures, i.e., in Eq. (8), $b$ is almost constant (while, if allowed to vary, $a$ shows small variations). For the standard Arrott plots, the gradients of the fitted straight lines vary significantly below $T_C$. This is a problem that is often overlooked in standard Arrott plots, as the critical amplitudes $a$ and $b$ in Eqs. (8) and (9) should be constants. Above $T_C$, $a$ and $b$ are found to vary significantly for both types of plot.

The Curie temperatures were calculated from both sets of plots by performing a linear fit to each isotherm and plotting the resulting $y$-intercepts against temperature. The sample $T_C$ values shown in Figs. 13(a) and 13(c) were calculated by fitting to the linear regions below the expected Curie temperatures. The resulting $T_C$ value for the 12% sample obtained from the three-dimensional Heisenberg plot is 183.5 K, while the value obtained from the $\beta$-Kouvel-Fisher plot is 183.7 K. This 0.2 K difference is consistent with the shift in $T_C$ apparent in Fig. 12(a) due to aging of the sample. The $T_C$ value for the 11% sample obtained from the three-dimensional Heisenberg plot is 169.1 K, while the value obtained from the

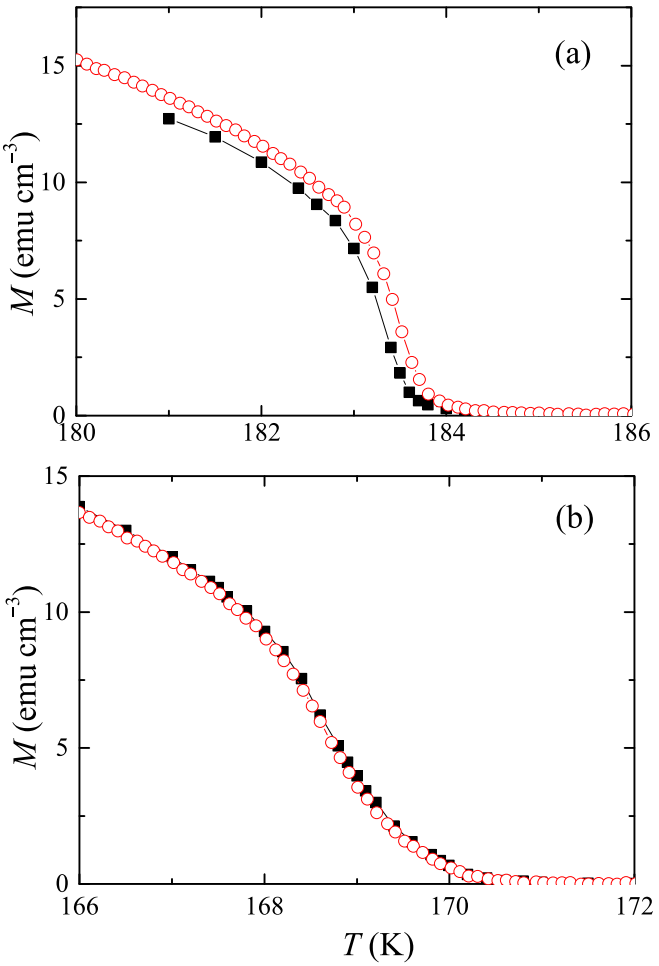


FIG. 12. (a) Thermoremnant magnetization for the 12% sample (red circles) and remanence obtained from $M$ vs $H$ hysteresis loops for the same sample some months later (black squares). (b) Same as (a) but for the 11% sample.

$\beta$-Kouvel-Fisher plot is 169.0 K. This 0.1 K difference is not significant given the uncertainties. The mean field Arrott plots produce $T_C$ values of 183.7 K and 169.4 K, which are only slightly higher than those obtained using three-dimensional Heisenberg exponents. Thus, even though these plots show that the behavior is significantly more consistent with three-dimensional Heisenberg behavior than mean field behavior, use of a standard (mean field) Arrott plots yield $T_C$ values close to the true values.

### G. Critical scaling plots

Figure 14 shows the scaling plots of the magnetic data for both samples using both the three-dimensional Heisenberg and mean field exponents, with relevant $T_C$ values obtained from the standard and modified Arrott plots, respectively. The data collapse roughly onto two branches corresponding to $T > T_C$ and $T < T_C$ over several orders of magnitude. For $T < T_C$, the scaling is slightly improved using Heisenberg rather than mean field exponents (compare in particular the upper curves in Figs. 14(a) and 14(b)). For example, fitting to a smooth curve for the data of 12% Mn sample yielded an adjusted $R$-squared value of 0.971 for the three-dimensional Heisenberg model and 0.888 for the mean field model. However, for $T > T_C$, the three-dimensional Heisenberg exponents do not give significantly better behavior than the mean field values. It is clear that one cannot determine the universality class or exponent values from our data using this type of plot.

### H. The critical exponent $\delta$

Figures 15(a) and 15(b) show $\log(M)$ against $\log(H)$ plots for a series of temperatures around $T_C$ for the two samples. The plots are reasonably linear close to the $T_C$ values obtained from the three-dimensional Heisenberg Arrott plots. Figures 15(c) and 15(d) show the dependence of the gradient of the log-log plots as a function of $T$. The value of $\delta$ obtained varies very rapidly with $T$, and one would need to know $T_C$ with a high degree of accuracy and confidence to obtain $\delta$ from such a plot. However, the values obtained are consistent with the three-dimensional Heisenberg value of 4.783 [33] at the $T_C$ values of 183.5 K and 169.1 K obtained from the three-dimensional Heisenberg Arrott plots. The plots are also significantly more linear at the three-dimensional Heisenberg value of $\delta$ than at the mean field value.

Using the experimental values of $\beta$ and $\gamma$ obtained from the Kouvel-Fisher plots and Eq. (5) gives $\delta = 5.0 \pm 0.2$ for both the 11% and 12% samples, which is consistent with the three-dimensional Heisenberg value of 4.783 [33].

### I. The critical exponent $\alpha$

As noted in Sec. II, close to $T_C$, the temperature derivative of resistivity should have the same power-law behavior as that of the specific heat in (Ga,Mn)As. We have demonstrated previously that there is indeed a peak in the temperature derivative of resistivity close to $T_C$ [18], but generally the peak is shifted to a temperature slightly below $T_C$ due to inhomogeneous broadening [19]. We find that even in our most homogeneous samples, the peak in the temperature derivative of resistivity is quite broad, and it is not possible to obtain meaningful values for the exponent $\alpha$ by fitting to the measured data.

Using the experimental values of $\beta$ and $\gamma$ obtained from the Kouvel-Fisher plots and Eq. (6) gives $\alpha = -0.19 \pm 0.07$ for the 12% sample and $\alpha = -0.25 \pm 0.10$ for the 11% sample. These values, which have large fractional uncertainties, are consistent with the three-dimensional Heisenberg value of $-0.133$ [33].

Yuldashev *et al.* [27] presented specific heat data for two (Ga,Mn)As samples. The samples were not annealed, and the measured remanent magnetization was found to vary quite slowly with temperature around the inferred $T_C$ values, as is typical for strongly inhomogeneous samples. Despite this, remarkably sharp cusps in the specific heat were observed at the inferred $T_C$ values, with the specific heat varying rapidly on temperature scales of $\sim 0.1$ K ($t \sim 0.002$). It is unclear how the observed behavior of the specific heat and the remanent magnetization can be consistent. Fitting to the observed specific heat for the two samples gives values of $\alpha = 0.09$ and 0.50 (without quoted uncertainties). These values are

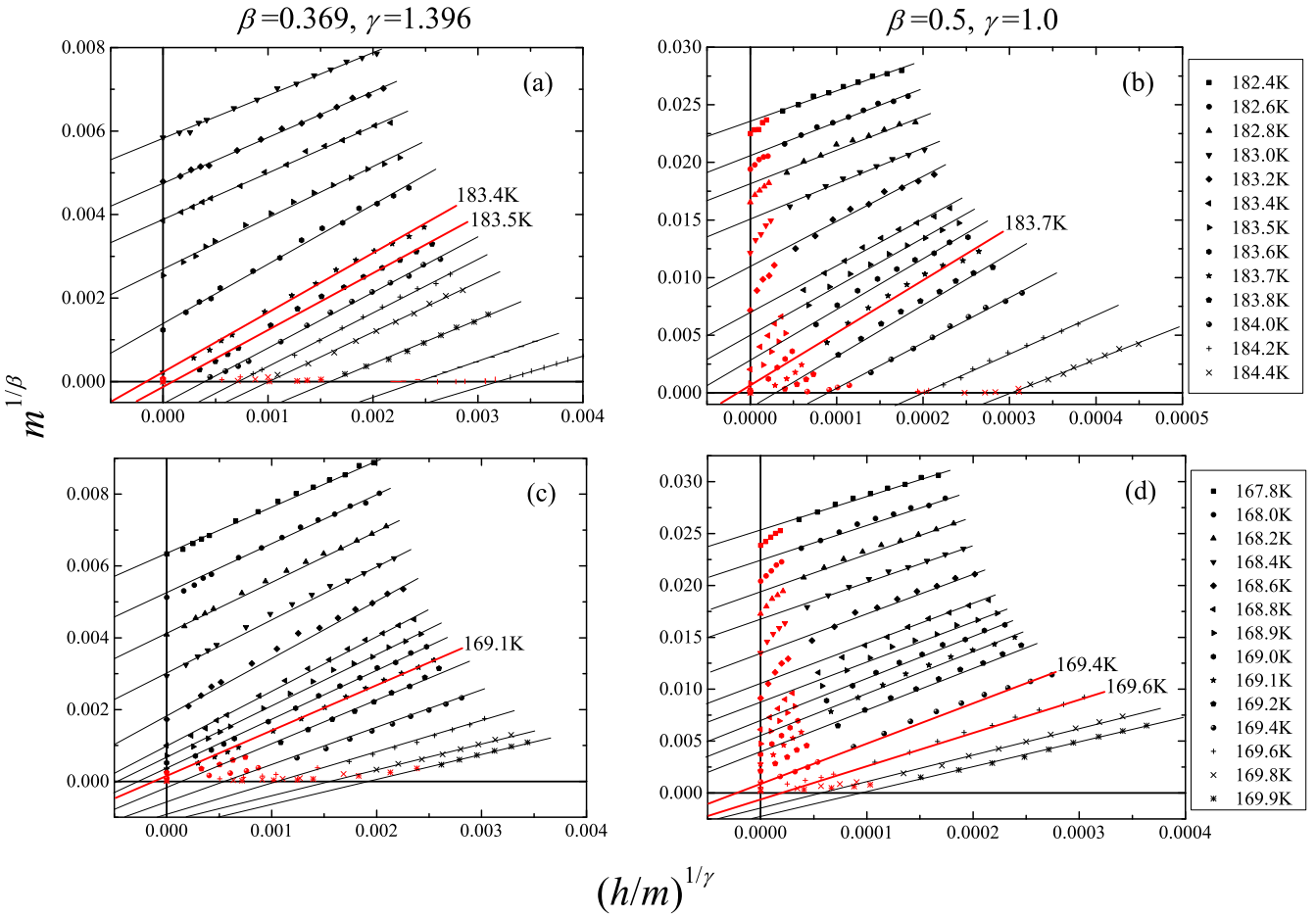


FIG. 13. Heisenberg modified Arrott plots for (a) 12% and (c) 11% Mn sample and standard mean field Arrott plots for (b) 12% and (d) 11% Mn sample. The straight lines in (a) and (c) are fits to the full data sets at each temperature. The straight lines in (b) and (d) are fits excluding the red points at low $h/m$.

inconsistent with both the three-dimensional Heisenberg value of $-0.133$ and the mean field value of 0.

## VI. COMPARISON WITH PREVIOUS PAPERS

As noted in Sec. I, most previous studies of critical behavior in (Ga,Mn)As have focused on the critical contribution to the resistivity close to $T_C$ [20]. The few experimental studies that have tried to determine critical exponents for (Ga,Mn)As [18,25–28] have produced imprecise and contradictory results.

Earlier papers, by some of the present authors and others, focused on the influence of scattering by critical fluctuations on the measured resistivity in (Ga,Mn)As. While demonstrating that the temperature derivative of resistivity had a clear maximum at $T_C$, in agreement with expectations [18,19], it was concluded that it was not possible to infer information about the universality class from the functional form of the temperature derivative of resistivity, which should follow that of the magnetic contribution to the specific heat. In an earlier paper by some of the present authors, an estimated value of $\beta$ of 0.3 to 0.4 [18], based on preliminary log-log plots, was given due to the problematic nature of this type of analysis, and the paper highlighted the need for a much more in-depth study of the critical region to obtain accurate exponent values. Khazen *et al.* [26] obtained a value of $\beta = 0.407$ based on a log-log plot analysis of magnetization data for (Ga,Mn)As. However, as pointed out in Sec. V C, the critical exponent in Ref. [26] was obtained by fitting down to $t = 0.35$ with a data point separation of 5 K, while we conclude that the upper limit of the accessible critical range is $t <\sim 0.025$. The value (but not the uncertainty, which is very small) quoted by Khazen *et al.* is consistent with the value we obtain below the critical range and does not provide information on critical behavior in (Ga,Mn)As.

Jiang *et al.* [25] attempted to obtain values of the critical exponents $\beta$ and $\gamma$ by measurements of anomalous Hall effect in a 2% Mn (Ga,Mn)As sample. They stated that their measurements provide strong evidence of mean field behavior in the sample studied. They inferred the behavior of magnetization and susceptibility by assuming that the anomalous Hall resistivity, $\rho_{xy}$, has the specific form

$$\rho_{xy} = C\rho_{xx}^{n} M. \tag{15}$$

It was further assumed that $C$ is a magnetic field– and temperature-independent constant and that $n = 2$. However, there are a series of problems with the approach used. (i) Generally the $n$ in Eq. (15) is system and disorder dependent, often having a value between 1 [46] and 2 [47].

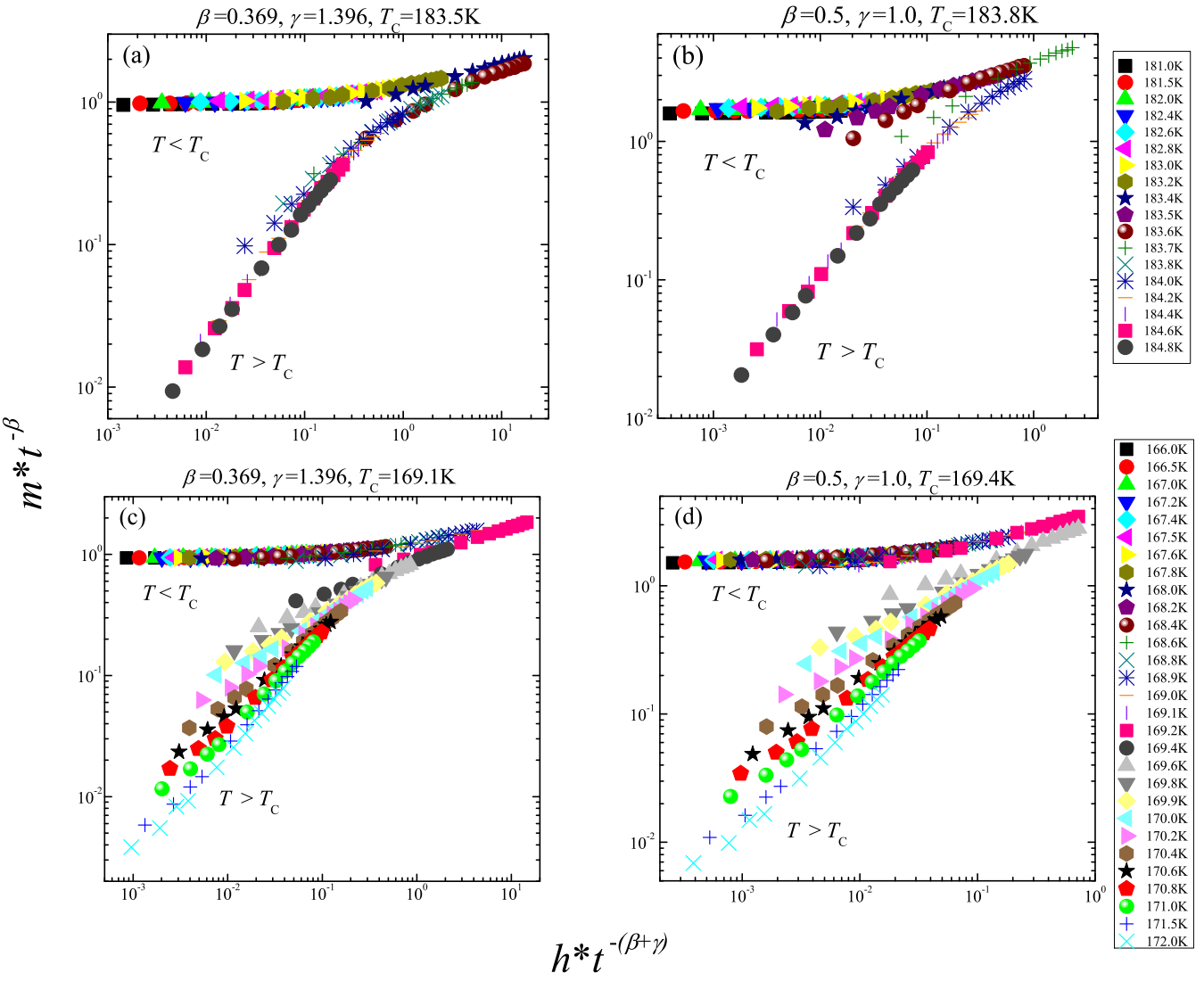


FIG. 14. Scaling plots for (a, b) 12% and (c, d) 11% Mn sample. (a) and (c) are for three-dimensional Heisenberg exponents, and (b) and (d) are for mean field exponents.

In measurements on (Ga,Mn)As, values between 0.4 and 2 have been reported [48]. Furthermore since the value of $n$ is dependent on scattering, it is possible for $n$ to also be a function of temperature. (ii) The magnetization in Eq. (15) is actually the component of the magnetization perpendicular to the thin (Ga,Mn)As film. Equation (15) therefore only gives the total magnetization when $M$ is saturated in the perpendicular direction. The sample used by Jiang *et al.* [25] had a strong in-plane magnetic anisotropy, so large fields were applied to rotate the magnetization out of plane. Fields greater than 3000 Oe were used to produce Arrott plots, which are far larger than those at which critical behavior can be expected to be observed. (iii) The temperature dependence of magnetization was inferred by extrapolation to zero applied field of the high field slope of *mean field* Arrott plots. (iv) Values of the critical exponents $\beta$ and $\gamma$ were obtained from log-log plots using these inferred magnetization values, but the data used were of low resolution, and the range of $|t|$ used for the power-law fitting was large. For example, for the $\beta$ plot, the two points closest to $T_C$ have $|t| \sim 0.05$ and 0.02, while for the $\gamma$ plot, the two points closest to $T_C$ have $|t| \sim 0.04$ and 0.01, so almost all the data used are probably outside of the critical range.

The results of Yuldashev *et al.* [27] on the specific heat data for two (Ga,Mn)As samples were discussed in Sec. V I. Values of $\alpha = 0.09$ and 0.50 (without quoted uncertainties) were obtained, which are inconsistent with both the three-dimensional Heisenberg value of $-0.133$ and the mean field value of 0. In this same paper, the $M(H)$ data "at $T_C$" for one of the samples were shown to vary as approximately $M^3 \sim H$. However, the data are again for large applied fields. On the basis of the seemingly contradictory results for the magnetization and the specific heat, these authors concluded that the behavior is suggestive of mean field behavior with Gaussian fluctuations. How the very sharp features in the specific heat could be consistent with the presence of significant spatial variations of the magnetization is unclear.

Stefanowicz *et al.* [29] studied the critical behavior of the related material (Ga,Mn)N. (Ga,Mn)N is a wide-bandgap magnetic semiconductor in which ferromagnetism arises

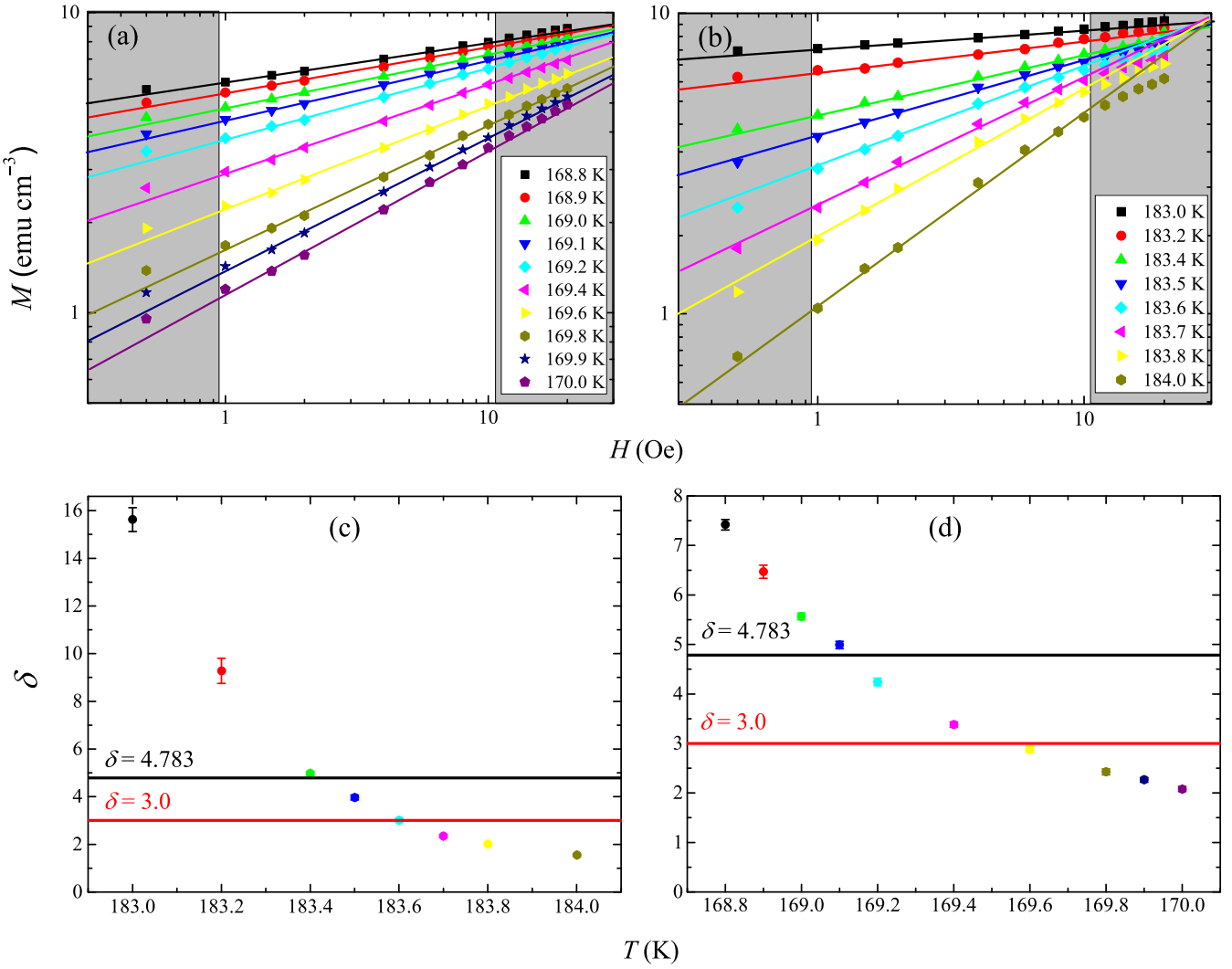


FIG. 15. Log-log plots of magnetization as a function of applied magnetic field close to $T_C$ for (a) 12% and (b) 11% Mn sample. Values of $\delta$ were obtained from fitting straight lines to the log-log plots in the range 1 to 10 Oe for (c) the 12% and (d) the 11% Mn sample.

from the very short-range superexchange interactions. They reported a significant smearing of the critical region, which was consistent with an inhomogeneous $T_C$ distribution with a $\Delta T_C$ of $0.4 \pm 0.2$ K ($t \sim \pm 0.04$). They found that $\beta_{\text{eff}}(t)$ and $\gamma_{\text{eff}}(t)$ vary rapidly and that no clear "critical range" could be identified. Fitting using Gaussian broadening with $\Delta T_C$, $\beta$, and $\gamma$ as free parameters gave $\beta = 0.6 \pm 0.1$ and $\gamma = 1.7 \pm 0.1$, which are far from the expected three-dimensional Heisenberg values. They suggested that this might be an indication of the effects of disorder and a breakdown of the Harris criteria or that the strong variation of $\beta$ and $\gamma$ might stem from the crossover from the large $|t|$ region (where both $\gamma$ and $\beta$ may be close to the mean field values) to the "true" critical region (sufficiently small $|t|$).

## VII. CONCLUSIONS

From detailed studies of the temperature- and magnetic field–dependent magnetization of thin epitaxial (Ga,Mn)As films with high Mn concentration, we conclude that accurate and reproducible values of the critical exponents $\beta$ and $\gamma$ can be obtained from Kouvel-Fisher plots only over a narrow range of temperatures. The strong intrinsic disorder present in dilute magnetic semiconductors places a limit on the temperature range over which critical behavior can be observed. We find that three-dimensional Heisenberg-like critical exponents are only obtained for absolute values of the reduced temperature $|t|$ below around 0.025. The accessible temperature range is further reduced by the presence of large length-scale inhomogeneity across the samples. Even in our most homogeneous samples, we find a $T_C$ broadening of around 0.4%, which limits the accessible critical region to around $0.025 > |t| > 0.005$.

For larger values of $|t|$, we observe apparent transitions of the critical exponent $\beta$ to values of around 0.4. This is consistent with the value obtained by Khazen *et al.* from fits to log-log plots of the magnetization as far as $|t| \approx 0.35$ [26]. We conclude that measurements obtained over such a wide temperature range do not provide information on critical behavior in (Ga,Mn)As.

We find that modified Arrott plots and scaling plots are not by themselves a practical way to determine the critical

exponents. The magnetic data are found to be in significantly better agreement with the Arrott-Noakes equation of state, using three-dimensional Heisenberg exponents, than with the mean field equation of state. The scaling plots of the magnetic data show the expected data collapse onto two branches corresponding to $T > T_C$ and $T < T_C$ over several orders of magnitude. However, similar behavior is observed using both three-dimensional Heisenberg and mean field exponents, and it was not found to be possible to draw significant conclusions about the universality class from these plots. We also find that determination of the critical exponent $\delta$ from $M(H,T_C)$ data is strongly dependent on an accurate knowledge of $T_C$. A value consistent with the three-dimensional Heisenberg exponent $\delta = 4.783$ is obtained using the critical temperature determined from modified Arrott plots, indicating self-consistency of the data set. Mean field Arrott plots produced from the same $M(H,T)$ data yield a slightly higher apparent $T_C$, which has a marked effect on the apparent value of $\delta$ obtained.

The measured values of the critical exponents $\beta$ and $\gamma$ are consistent with the three-dimensional Heisenberg values and are inconsistent with the mean field or modified mean field behavior claimed in previous publications. Furthermore, measurements of $M(H)$ close to $T_C$ are consistent with the three-dimensional Heisenberg values of the critical exponent $\delta$. We therefore conclude that the critical behavior of (Ga,Mn)As is that of the three-dimensional Heisenberg class despite the very strong site disorder.

## ACKNOWLEDGMENTS

We acknowledge funding from European Union Grant No. FP7-214499–NAMASTE, European Research Council Advanced Grant No. 268066, and The Engineering and Physical Sciences Research Council Grant No. EP/H002294. We are grateful to Tomas Jungwirth, Vit Novak, Maciek Sawicki, and Tomasz Dietl for useful discussions.

[1] J. J. Binney, N. J. Dowrick, A. J. Fisher, and M. E. J. Newman, *The Theory of Critical Phenomena* (Oxford Science Publications, Oxford, 1992).

[2] M. E. Fisher, S.-K. Ma, and B. G. Nickel, Phys. Rev. Lett. **29**, 917 (1972).

[3] A. Aharony, in *Phase Transitions and Critical Phenomena*, edited by C. Domb and M. S. Green (Academic Press, New York, 1976), Vol. 6, pp. 357–424.

[4] A. B. Harris and T. C. Lubensky, Phys. Rev. Lett. **33**, 1540 (1974).

[5] A. Gordillo-Guerrero and J. J. Ruiz-Lorenzo, J. Stat. Mech. (2007) P06014, and references therein.

[6] M. Dudka, R. Folk, Yu. Holovatch, and D. Ivaneiko, J. Magn. Magn. Mater. **256**, 243 (2003), and references therein.

[7] D. J. Priour, Jr. and S. Das Sarma, Phys. Rev. B **81**, 224403 (2010).

[8] H. Ohno, A. Shen, F. Matsukura, A. Oiwa, A. Endo, S. Katsumoto, and Y. Iye, Appl. Phys. Lett. **69**, 363 (1996).

[9] T. Jungwirth, J. Wunderlich, V. Novák, K. Olejník, B. L. Gallagher, R. P. Campion, K. W. Edmonds, A. W. Rushforth, A. J. Ferguson, and P. Němec, Rev. Mod. Phys. **86**, 855 (2014).

[10] T. Jungwirth, B. L. Gallagher, and J. Wunderlich, in *Semiconductors and Semimetals*, edited by E. R. Weber (Elsevier, Amsterdam, 2008), Vol. 82, Chap. 4, pp. 135–205.

[11] T. Dietl and H. Ohno, Rev. Mod. Phys. **86**, 187 (2014).

[12] H. Ohno, D. Chiba, F. Matsukura, T. Omiya, E. Abe, T. Dietl, Y. Ohno, and K. Ohtani, Nature **408**, 944 (2000); D. Chiba, M. Yamanouchi, F. Matsukura, and H. Ohno, Science **301**, 943 (2003).

[13] C. Ruster, T. Borzenko, C. Gould, G. Schmidt, L. W. Molenkamp, X. Liu, T. J. Wojtowicz, J. K. Furdyna, Z. G. Yu, and M. E. Flatte, Phys. Rev. Lett. **91**, 216602 (2003); C. Gould, C. Ruster, T. Jungwirth, E. Girgis, G. M. Schott, R. Giraud, K. Brunner, G. Schmidt, and L. W. Molenkamp, *ibid.* **93**, 117203 (2004); A. D. Giddings, M. N. Khalid, T. Jungwirth, J. Wunderlich, S. Yasin, R. P. Campion, K. W. Edmonds, J. Sinova, K. Ito, K.-Y. Wang, D. Williams, B. L. Gallagher, and C. T. Foxon, *ibid.* **94**, 127202 (2005).

[14] M. Yamanouchi, D. Chiba, F. Matsukura, and H. Ohno, Nature **428**, 539 (2004); D. Chiba, Y. Sato, T. Kita, F. Matsukura, and H. Ohno, Phys. Rev. Lett. **93**, 216602 (2004).

[15] E. De Ranieri, P. E. Roy, D. Fang, E. K. Vehsthedt, A. C. Irvine, D. Heiss, A. Casiraghi, R. P. Campion, B. L. Gallagher, T. Jungwirth, and J. Wunderlich, Nat. Mater. **12**, 808 (2013).

[16] Y. Ohno, D. K. Young, B. Beschoten, F. Matsukura, H. Ohno, and D. D. Awschalom, Nature **402**, 790 (1999).

[17] M. Wang, R. P. Campion, A. W. Rushforth, K. W. Edmonds, C. T. Foxon, and B. L. Gallagher, Appl. Phys. Lett. **93**, 132103 (2008).

[18] V. Novak, K. Olejnik, J. Wunderlich, M. Cukr, K. Vyborny, A. W. Rushforth, K. W. Edmonds, R. P. Campion, B. L. Gallagher, J. Sinova, and T. Jungwirth, Phys. Rev. Lett. **101**, 077201 (2008).

[19] M. Wang, K. W. Edmonds, B. L. Gallagher, A. W. Rushforth, O. Makarovsky, A. Patane, R. P. Campion, C. T. Foxon, V. Novak, and T. Jungwirth, Phys. Rev. B **87**, 121301 (2013).

[20] A. Van Esch, L. Van Bockstal, J. De Boeck, G. Verbanck, A. S. van Steenbergen, P. J. Wellmann, B. Grietens, R. Bogaerts, F. Herlach, and G. Borghs, Phys. Rev. B **56**, 13103 (1997); F. Matsukura, H. Ohno, A. Shen, and Y. Sugawara, *ibid.* **57**, R2037(R) (1998); T. Omiya, F. Matsukura, T. Dietl, Y. Ohno, T. Sakon, M. Motokawa, and H. Ohno, Physica E **7**, 976 (2000); P. Kuivalainen, Phys. Status Solidi B **227**, 449 (2001); Sh. U. Yuldashev, Hyunsik Im, V. Sh. Yalishev, C. S. Park, T. W. Kang, Sanghoon Lee, Y. Sasaki, X. Liu, and J. K. Furdyna, Appl. Phys. Lett. **82**, 1206 (2003); M. P. López-Sancho and L. Brey, Phys. Rev. B **68**, 113201 (2003); C. Timm, M. E. Raikh, and F. von Oppen, Phys. Rev. Lett. **94**, 036602 (2005); C. P. Moca, B. L. Sheu, N. Samarth, P. Schiffer, B. Janko, and G. Zarand, *ibid.* **102**, 137203 (2009); T. Dietl, J. Phys. Soc. Jpn. **77**, 031005 (2008).

[21] P. G. de Gennes and J. Friedel, J. Phys. Chem. Solids **4**, 71 (1958); C. Haas, Crit. Rev. Solid State Sci. **1**, 47 (1970).

[22] M. Wang, R. A. Marshall, K. W. Edmonds, A. W. Rushforth, R. P. Campion, and B. L. Gallagher, Appl. Phys. Lett. **104**, 132406 (2014).

[23] L. W. Shacklette, Phys. Rev. B **9**, 3789 (1974); P. P. Craig, W. I. Goldburg, T. A. Kitchens, and J. I. Budnick, Phys. Rev. Lett. **19**, 1334 (1967).
[24] D. Kim, B. L. Zink, F. Hellman, S. McCall, G. Cao, and J. E. Crow, Phys. Rev. B **67**, 100406(R) (2003).
[25] W. Jiang, A. Wirthmann, Y. S. Gui, X. Z. Zhou, M. Reinwald, W. Wegscheider, C.-M. Hu, and G. Williams, Phys. Rev. B **80**, 214409 (2009).
[26] Kh. Khazen, H. J. von Bardeleben, J. L. Cantin, A. Mauger, L. Chen, and J. H. Zhao, Phys. Rev. B **81**, 235201 (2010).
[27] S. U. Yuldashev, K. T. Igamberdiev, S. Lee, Y. Kwon, T. W. Kang, and A. G. Shashkov, J. Korean Phys. Soc. **59**, 431 (2011).
[28] S. Yuldashev, K. Igamberdiev, S. Lee, Y. Kwon, Y. Kim, H. Im, A. Shashkov, and T. W. Kang, Appl. Phys. Express **3**, 073005 (2010).
[29] S. Stefanowicz, G. Kunert, C. Simserides, J. A. Majewski, W. Stefanowicz, C. Kruse, S. Figge, T. Li, R. Jakieła, K. N. Trohidou, A. Bonanni, D. Hommel, M. Sawicki, and T. Dietl, Phys. Rev. B **88**, 081201(R) (2013).
[30] T. Dietl, H. Ohno, and F. Matsukura, Phys. Rev. B **63**, 195205 (2001); M. Abolfath, T. Jungwirth, J. Brum, and A. H. MacDonald, *ibid.* **63**, 054418 (2001).
[31] S. Piano, X. Marti, A. W. Rushforth, K. W. Edmonds, R. P. Campion, M. Wang, O. Caha, T. U. Schulli, V. Holy, and B. L. Gallagher, Appl. Phys. Lett. **98**, 152503 (2011); M. Kopecký, J. Kub, F. Máca, J. Mašek, O. Pacherová, A. W. Rushforth, B. L. Gallagher, R. P. Campion, V. Novák, and T. Jungwirth, Phys. Rev. B **83**, 235324 (2011); M. Birowska, C. Sliwa, J. A. Majewski, and T. Dietl, Phys. Rev. Lett. **108**, 237203 (2012).
[32] K.-Y. Wang, M. Sawicki, K. W. Edmonds, R. P. Campion, S. Maat, C. T. Foxon, B. L. Gallagher, and T. Dietl, Phys. Rev. Lett. **95**, 217204 (2005).
[33] M. Campostrini, M. Hasenbusch, A. Pelissetto, P. Rossi, and E. Vicari, Phys. Rev. B **65**, 144520 (2002); A. Pelissettoa and E. Vicari, Phys. Rep. **368**, 549 (2002).
[34] A. Arrott and J. E. Noakes, Phys. Rev. Lett. **19**, 786 (1967).
[35] M. D. Kuz'min and A. M. Tishin, Europhys. Lett. **73**, 396 (2006).
[36] A. Arrott, Phys. Rev. **108**, 1394 (1957).
[37] L. Chen, X. Yang, F. Yang, J. H. Zhao, J. Misuraca, P. Xiong, and S. von Molnar, Nano Lett. **11**, 2584 (2011).
[38] J. S. Kouvel and M. E. Fisher, Phys. Rev. **136**, A1626 (1964).
[39] P. Nemec, V. Novak, N. Tesarova, E. Rozkotova, H. Reichlova, D. Butkovicova, F. Trojanek, K. Olejnk, P. Maly, R. P. Campion, B. L. Gallagher, Jairo Sinova, and T. Jungwirth, Nat. Commun. **4**, 1422 (2013).
[40] K. W. Edmonds, P. Boguslawski, K. Y. Wang, R. P. Campion, S. N. Novikov, N. R. S. Farley, B. L. Gallagher, C. T. Foxon, M. Sawicki, T. Dietl, M. BuongiornoNardelli, and J. Bernholc, Phys. Rev. Lett. **92**, 037201 (2004).
[41] T. Jungwirth, J. Masek, K. Y. Wang, K. W. Edmonds, M. Sawicki, M. Polini, Jairo Sinova, A. H. MacDonald, R. P. Campion, L. X. Zhao, N. R. S. Farley, T. K. Johal, G. van der Laan, C. T. Foxon, and B. L. Gallagher, Phys. Rev. B **73**, 165205 (2006).
[42] O. Proselkov, D. Sztenkiel, W. Stefanowicz, M. Aleszkiewicz, J. Sadowski, T. Dietl, and M. Sawicki, Appl. Phys. Lett. **100**, 262405 (2012).
[43] B. J. Kirby, J. A. Borchers, J. J. Rhyne, S. G. E. te Velthuis, A. Hoffmann, K. V. O'Donovan, T. Wojtowicz, X. Liu, W. L. Lim, and J. K. Furdyna, Phys. Rev. B **69**, 081307 (2004).
[44] F. Bloch, Z. Physik **61**, 206 (1930).
[45] M. Sperl, A. Singh, U. Wurstbauer, S. K. Das, A. Sharma, M. Hirmer, W. Nolting, C. H. Back, W. Wegscheider, and G. Bayreuther, Phys. Rev. B **77**, 125212 (2008).
[46] J. Smit, Physica **21**, 877 (1955); **24**, 39 (1958).
[47] L. Berger, Phys. Rev. B **2**, 4559 (1970); T. Jungwirth, Q. Niu, and A. H. MacDonald, Phys. Rev. Lett. **88**, 207208 (2002).
[48] K. W. Edmonds, K. Y. Wang, R. P. Campion, A. C. Neumann, C. T. Foxon, B. L. Gallagher, and P. C. Main, Appl. Phys. Lett. **81**, 3010 (2002); S. H. Chun, Y. S. Kim, H. K. Choi, I. T. Jeong, W. O. Lee, K. S. Suh, Y. S. Oh, K. H. Kim, Z. G. Khim, J. C. Woo, and Y. D. Park, Phys. Rev. Lett. **98**, 026601 (2007); M. Glunk, J. Daeubler, W. Schoch, R. Sauer, and W. Limmer, Phys. Rev. B **80**, 125204 (2009).